3. A. C. Chan, D. M. Desai, A. Weiss, *Annu. Rev. Immunol.* **12**, 555 (1994).
4. A. Rao and P. G. Hogan, *ibid.* **15**, 707 (1997).
5. B. S. Skalhegg *et al.*, *Science* **263**, 84 (1994); D. Laxminarayana and G. M. Kammer, *J. Immunol.* **156**, 497 (1996).
6. M. R. Vossler *et al.*, *Cell* **89**, 73 (1997).
7. T. J. Novak and E. V. Rothenberg, *Proc. Natl. Acad. Sci. U.S.A.* **87**, 9353 (1990); Y. P. Hsueh and M. Z. Lai, *J. Biol. Chem.* **270**, 18094 (1995); A. Tamir, Y. Granot, N. Isakov, *J. Immunol.* **157**, 1514 (1996); E. M. Aandahl *et al.*, *FASEB J.* **12**, 855 (1998).
8. L. Tsuruta *et al.*, *J. Immunol.* **154**, 5255 (1995); C. R. Beals, C. M. Sheridan, C. W. Turck, P. Gardner, G. R. Crabtree, *Science* **275**, 1930 (1997); C. M. Sheridan and P. Gardner, paper presented at the Gordon Research Conferences, Kimball Union, NH, 7 June 1998.
9. J. Marx, *Science* **262**, 988 (1993); J. Wu *et al.*, *ibid.*, p. 1065; H. Mischak *et al.*, *Mol. Cell Biol.* **16**, 5409 (1996); A. B. Sprenkle, S. P. Davies, D. Carling, D. G. Hardie, T. W. Sturgill, *FEBS Lett.* **403**, 254 (1997).
10. J. A. Beavo, *Physiol. Rev.* **75**, 725 (1995).
11. T. J. Bloom and J. A. Beavo, *Proc. Natl. Acad. Sci. U.S.A.* **93**, 14188 (1996).
12. L. Li and J. A. Beavo, unpublished data.
13. S. A. Robicsek *et al.*, *Biochem. Pharmacol.* **42**, 869 (1991); M. A. Giembycz, C. J. Corrigan, J. Seybold, R. Newton, P. J. Barnes, *Br. J. Pharmacol.* **118**, 1945 (1996).
14. J. Seybold *et al.*, *J. Biol. Chem.* **273**, 20575 (1998).
15. T. Michaeli *et al.*, *ibid.* **268**, 12925 (1993); P. Han, X. Zhu, T. Michaeli, *ibid.* **272**, 16152 (1997).
16. For the protein immunoblot analysis, 20 μg of total protein was loaded in each lane and separated with 8% SDS–polyacrylamide gel electrophoresis. Affinity-purified antibody 6858 to PDE7, diluted with phosphate-buffered saline (PBS) containing 5% nonfat milk, was used for protein immunoblot analysis. Specific protein bands were revealed by the ECL system (Pierce, IL). For the immunoprecipitation and PDE assay, 10 million isolated peripheral T cells were homogenized with 1 ml of 40 mM tris-HCl buffer (homogenizing buffer) containing 1 mM EDTA, 5 mM dithiothreitol, 1 μM pepstatin (Sigma), and 10 μM leupeptin (Sigma). After centrifugation for 20 min at 14,000 rpm (Microcentrifuge), the supernatant was saved and was incubated overnight at 4°C with 100 μl of affinity-purified antibody 6858. Protein A–Sepharose (200 μl of a 5% suspension) was then added, and the mixture was incubated for 3 hours at 4°C. The protein A–bound proteins were washed twice with PBS and resuspended with the homogenization buffer for measurement of PDE activity, using 1 μM cAMP as a substrate. For the radioimmunoassay of cAMP, cells were homogenized in 5% trichloroacetic acid according to the protocol provided with the radioimmunoassay system (NEN, Boston, MA). To measure proliferation, cells (10^5 cells per well) were plated in a 96-well plate precoated with goat antibodies to mouse IgG and were incubated with anti-CD3 or anti-CD28 or both for 8 hours. One microcurie of [^{3}H]thymidine was then added per well. Sixteen hours later, cells were harvested for scintillation counting.
17. The three PDE7 antisense oligonucleotides were as follows: from position 1 to 24 (AS-0: 5′-CGGCAGCTGCTAACACACTTCCAT); from position 708 to 728 (AS-708: 5′-CAGTGCATGGCCTGAGTAAC); and from position 937 to 959 (AS-959: 5′-GGCAGATGTGAGAATAAGCCTG). For RT-PCR analysis, PDE7-specific primer pairs were as follows: 5′-GATATTTGTAACCCATGTCGGACG-3′ and 5′-AAAGCTTGGCGGTACTCTATCGAT-3′. PDE4A-specific primer pairs were as follows: AAGAGGAGGAAGAAATATCAATGG and TTACAGCAACCACGAATTCCTCC.
18. We thank L. H. Li for help with RT-PCR analysis and D. Stenger for comments on the manuscript. This research is supported by NIH grant DK21723 to J.A.B. and by a grant from the Ono Pharmaceutical Company. C.Y. is the recipient of a Career Award from the Burroughs Wellcome Fund.

13 October 1998; accepted 5 January 1999

Requirement of Cdk2–Cyclin E Activity for Repeated Centrosome Reproduction in *Xenopus* Egg Extracts

Edward H. Hinchcliffe,[1]* Chuan Li,[2]* Elizabeth A. Thompson,[1] James L. Maller,[2] Greenfield Sluder[1]†

The abnormally high number of centrosomes found in many human tumor cells can lead directly to aneuploidy and genomic instability through the formation of multipolar mitotic spindles. To facilitate investigation of the mechanisms that control centrosome reproduction, a frog egg extract arrested in S phase of the cell cycle that supported repeated assembly of daughter centrosomes was developed. Multiple rounds of centrosome reproduction were blocked by selective inactivation of cyclin-dependent kinase 2–cyclin E (Cdk2-E) and were restored by addition of purified Cdk2-E. Confocal immunomicroscopy revealed that cyclin E was localized at the centrosome. These results demonstrate that Cdk2-E activity is required for centrosome duplication during S phase and suggest a mechanism that could coordinate centrosome reproduction with cycles of DNA synthesis and mitosis.

In animal cells, the interphase centrosome reproduces or duplicates only once per cell cycle, thereby ensuring a strictly bipolar mitotic spindle axis (*1*). Because there is no cell cycle checkpoint that monitors the number of spindle poles (*2*), uncontrolled duplication of the centrosome can contribute to genomic instability through the formation of multipolar mitotic spindles. Indeed, many human tumor cells, including those lacking the tumor suppresser protein p53 (*3*), have abnormally high numbers of centrosomes (*4*).

Studies of sea urchin and *Xenopus* embryos and clam oocyte lysates have revealed that the centrosome cycle can be regulated solely by cytoplasmic mechanisms (*5*–*8*): The repeated duplication of the centrosome proceeds in the complete absence of either a nucleus (*7*) or protein synthesis (*8*). In theory, the cyclical rise and fall in the activity of one or more cyclin-dependent kinases (Cdks) could be the cytoplasmic mechanism that coordinates centrosome reproduction with cell cycle progression. However, the fact that centrosomes repeatedly duplicate in the complete absence of protein synthesis indicates that the activities of those Cdks that are dependent on the translation of their cyclin subunits during each cell cycle (that is, Cdk1–cyclin A or –cyclin B or both) do not regulate centrosome reproduction or assembly (*8*). Nevertheless, Cdk2–cyclin E (Cdk2-E) remains a potential candidate to control centrosome duplication and coordinate it with nuclear events during the cell cycle (*6*, *9*, *10*). Cdk2-E activity drives the transition from G_1 to S phase in somatic cells (*11*), which is the time during the cell cycle when daughter centrosome assembly is thought to begin (*12*). Importantly, in early *Xenopus* embryos, Cdk2-E activity is not dependent on the synthesis and degradation of the cyclin E subunit, as the amount of cyclin E remains constant until the mid-blastula transition (MBT) (*13*).

To investigate whether Cdk2-E activity regulates centrosome duplication, we developed an S phase–arrested *Xenopus* egg extract that supports repeated centrosome reproduction in vitro. We used an S phase extract because centrosomes will undergo multiple rounds of duplication during S phase arrest in both zygotes and somatic cells (*6*, *8*, *14*, *15*). Unlike cycling extracts, Cdk2-E activity can be inhibited in S phase–arrested extracts without the concern that this inhibition will block cell cycle progression at a point before centrosomes are normally scheduled to reproduce. To make these extracts, we prepared a cycling *Xenopus* egg extract (*16*, *17*) and then added aphidicolin, an inhibitor of α-DNA polymerase (*18*), and demembranated *Xenopus* sperm nuclei (*19*). Histone H1 kinase activity in control extracts cycled at least twice with a cell cycle time of ~50 min; in contrast, H1 activity in aphidicolin-treated extracts remained at a constant, low amount for 6 hours (*20*, *21*). Time-lapse videomicroscopy of aphidicolin-treated extracts revealed that nuclear envelope breakdown did not occur during the 6-hour experiment (*20*). Thus,

[1]Department of Cell Biology, University of Massachusetts Medical School, Worcester, MA 01605, USA. [2]Howard Hughes Medical Institute and Department of Pharmacology, University of Colorado School of Medicine, Denver, CO 80262, USA.

*These authors contributed equally to this work.
†To whom correspondence should be addressed. E-mail: Greenfield.Sluder@ummed.edu

our extracts are arrested in S phase because of the activation of the cell cycle checkpoint that monitors the completion of DNA synthesis.

We characterized the pattern of centrosome reproduction in aphidicolin-treated extracts with time-lapse videomicroscopy. We used polarization optics to directly visualize the astral microtubules organized by the sperm centrosomes and found that aster number increased over 6 hours (Fig. 1A). Because *Xenopus* extracts do not spontaneously assemble microtubule asters or centrosomes in the absence of added sperm nuclei (*22*), this increase in aster number indicates centrosome doubling. The total number of asters in the field eventually declined, because some asters moved out of the plane of focus or off the field of view (Fig. 1A, panel d). Figure 1B shows an individual aster from another extract that doubled three times, its daughters remaining fortuitously close together and in the plane of focus.

We analyzed the pattern of doubling for all asters in a given field in aphidicolin-treated extracts and scored those that had at least one first, second, or third generation daughter aster visible for the duration of the 6-hour experiment. Of the individual asters for which we obtained a complete lineage analysis ($N = 59$), 5% completed four rounds of duplication, 69% underwent three rounds, 14% showed two rounds, 2% showed a single round, and 10% did not duplicate. Asters whose progeny were all lost from view during the experiment were not included. Nevertheless, Table 1 shows the complete data set for aster duplication at each successive round, regardless of whether or not individual asters subsequently became lost from the field. The multiple rounds of aster doubling in a strict one-to-two fashion at each cycle (Fig. 1B) are characteristic of complete centrosome reproduction and cannot be explained by either centrosome splitting or fragmentation of the microtubule organizing center (*23*). Together, our results define a cell-free system that allows the real-time observation of the complete centrosome reproductive cycle in vitro.

To directly test whether Cdk2-E activity was required for repeated centrosome reproduction during S phase arrest, we selectively inactivated Cdk2-E by addition of recombinant Δ34Xic1, a 34–amino acid NH_2-terminus truncated variant of $Xic1^{p27}$, a *Xenopus* cdk inhibitor (*24*, *25*). Δ34Xic1 inhibits the activity of Cdk2-E with a median inhibitory concentration (IC_{50}) value of 10 nM and only affects Cdk1–cyclin A and –cyclin B activity at higher concentrations (IC_{50} = 5 μM) (*24*). Because Cdk2 does not complex with cyclin A until after the MBT (*9*, *13*, *26*), Cdk2–cyclin A activity was not a factor in this study. Inhibition of Cdk2-E does not drive the cell cycle out of S phase because the majority of S phase–promoting activity is provided by Cdk1–cyclin A (*26*), which is not inhibited in vitro by Δ34Xic1 at the concentration used here (*9*, *24*).

Extracts were prepared and split into two portions. To the first of these, C-Xic1 (the COOH-terminal half of Xic1) was added as a control because it does not affect the activity of Cdk2-E in vitro (*9*, *24*). To the second portion, we added Δ34Xic1 (175 nM final concentration) and then separated this sample into two further portions. To the first of these, buffer was added, and to the second, we added an equal volume of baculovirus-ex-

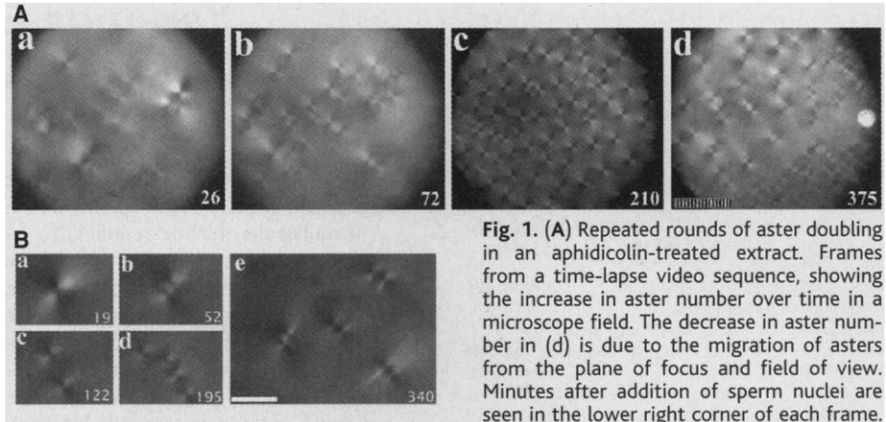

Fig. 1. (**A**) Repeated rounds of aster doubling in an aphidicolin-treated extract. Frames from a time-lapse video sequence, showing the increase in aster number over time in a microscope field. The decrease in aster number in (d) is due to the migration of asters from the plane of focus and field of view. Minutes after addition of sperm nuclei are seen in the lower right corner of each frame. Polarization optics. Ten micrometers per scale division. (**B**) Time-lapse sequence showing an individual aster from another aphidicolin-treated extract undergoing three rounds of doubling. (a) The aster at the start of the time-lapse sequence. (b and c) Doubling of this aster and separation of the daughter asters. (d) Doubling of these daughters. (e) Third round of doubling yields eight asters. Minutes after addition of sperm nuclei are seen in the lower right corner of each frame. Polarization optics. Bar in (e), 10 μm.

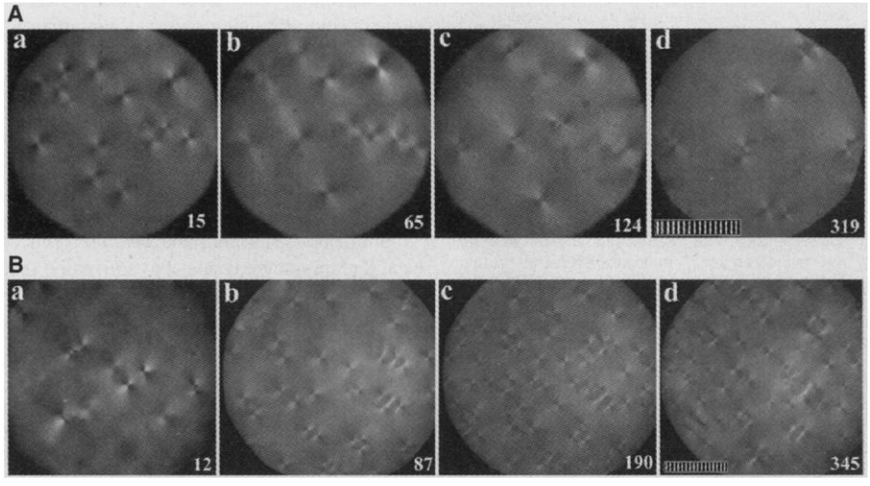

Fig. 2. (**A**) Selectively inhibiting Cdk2-E activity blocks repeated centrosome reproduction. Time-lapse sequence showing one round of aster doubling in an aphidicolin-treated extract containing 175 nM Δ34Xic1. Minutes after addition of sperm nuclei are seen in the lower right corner of each frame. Polarization optics. Ten micrometers per scale division. (**B**) Time-lapse sequence showing the restoration of multiple rounds of aster doubling in an aphidicolin-treated extract containing 175 nM Δ34Xic1 plus 245 nM Cdk2-E. Minutes after addition of sperm nuclei are seen in the lower right corner of each frame. Polarization optics. Ten micrometers per scale division.

Table 1. Aphidicolin-treated extracts followed for 6 hours.

Round of duplication	Starting number of asters at each round	Number of asters lost*	Number that remain	Number and percentage that duplicate
First	62	2	60	57 (95%)
Second	114	19	95	91 (96%)
Third	182	76	106	70 (66%)
Fourth	140	37	103	4 (4%)

*This is the number of asters that moved out of the plane of focus or off the field of view before they doubled.

pressed, affinity-purified active Cdk2-E complex (245 nM final concentration, equal to 1.4 times the molar amount of Δ34Xic1 added) (*9*, *13*, *24*, *27*). The pattern of aster doubling under each of these three conditions was then simultaneously recorded with separate videomicroscopy systems (Fig. 2, A and B).

Analysis of the behavior of the asters in extracts treated with Xic1-C (N = 31 asters) revealed that 77% of the asters completed three rounds of doubling and 23% doubled twice. In the Δ34Xic1-treated extracts, 6% of the asters (N = 53) failed to double at all, 79% doubled only once, 15% doubled twice, and none doubled three times over 6 hours.

When purified active Cdk2-E was added back to Δ34Xic1-treated extracts, 50% of the asters (N = 52) underwent two and 42% underwent three rounds of duplication, whereas only 8% of the asters doubled just once over 6 hours. Table 2 shows the complete data set for all asters followed under these three conditions regardless of whether any daughter asters subsequently became lost from view. These results reveal that the activity of Cdk2-E is required for centrosomes to undergo repeated reproduction during S phase arrest.

We characterized the localization of cyclin E in *Xenopus* embryonic blastomeres by confocal immunofluorescence microscopy, using an affinity-purified antibody to cyclin E (*9*, *28*). Cyclin E was found to be distributed diffusely throughout the cytoplasm but showed maximal concentration at the centrosome region (Fig. 3). Thus, the Cdk2-E complex may become accumulated at the centrosome, as has been reported for other Cdk-cyclin complexes (*29*).

Previously, it was demonstrated that only a single round of daughter centrosome assembly can occur in sea urchin zygotes arrested before the onset of S phase, whereas repeated rounds of duplication occur during S phase arrest (*6*). Thus, the morphological events of daughter centrosome assembly can occur before the G_1-S transition, but entry into S phase appears to be necessary for the centrosome to duplicate again. This suggests that a "licensing" event during S phase restores the reproductive capacity to the daughter centrosomes, thereby permitting them to duplicate again during the next cell cycle. Here, our finding that the inactivation of Cdk2-E does not inhibit the first round of aster doubling in vitro, but does block further rounds (Fig. 2A and Table 2), suggests that the daughter centrosomes cannot reduplicate in the absence of Cdk2-E activity. Perhaps Cdk2-E is the "licensing" factor that restores the reproductive capacity to the daughter centrosomes. In this regard, it is important to determine if the abnormal centrosome number observed in both mouse embryonic fibroblasts lacking p53 (*3*) and many human tumor cells (*4*) is due to the misregulation of Cdk2-E activity at the G_1-S transition and during S phase.

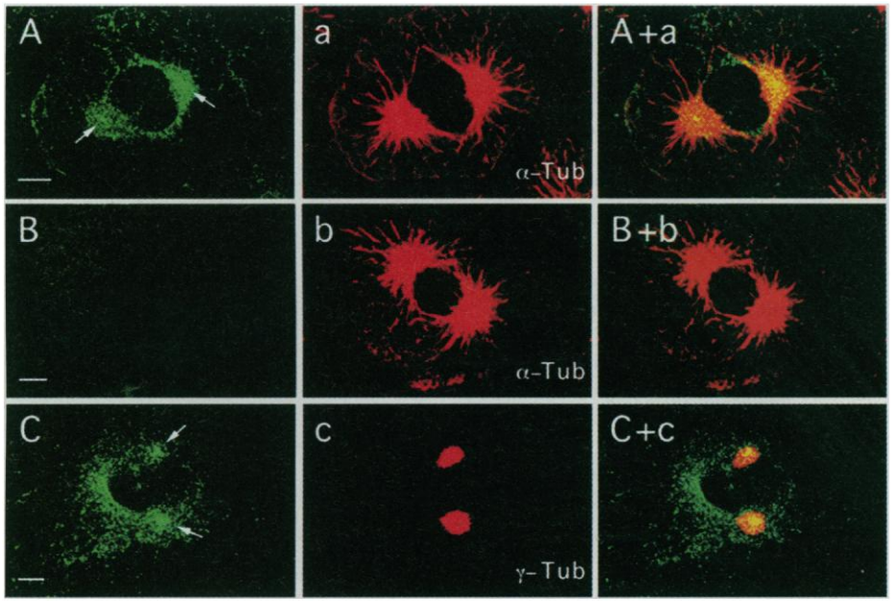

Fig. 3. Localization of cyclin E in *Xenopus* embryonic blastomeres by immunofluorescence microscopy. Shown are three separate cells double immunostained with antibody to cyclin E (**A** through **C**) and antibody to α tubulin (α-Tub) (a and b) or antibody to γ tubulin (γ-Tub) (c). In (B), the antibody to cyclin E was preabsorbed to the initial cyclin E antigen. A + a, B + b, and C + c represent merged images. Centromeres are marked by arrows (A and C). Confocal microscopy. Bars in (A), (B), and (C), 10 μm.

Table 2. Aphidicolin-treated extracts followed for 6 hours.

Round of duplication	Starting number of asters at each round	Number of asters lost*	Number that remain	Number and percentage that duplicate
		Xic1-C		
First	34	0	34	34 (100%)
Second	68	15	53	53 (100%)
Third	106	33	73	46 (63%)
		Δ34Xic1		
First	64	8	56	53 (95%)
Second	106	20	86	10 (12%)
Third	20	1	19	0 (0%)
		Δ34Xic1 + Cdk2-E		
First	56	0	56	56 (100%)
Second	112	12	100	91 (91%)
Third	182	46	136	43 (68%)

*This is the number of asters that moved out of the plane of focus or off the field of view before they doubled.

References and Notes

1. D. Mazia, *Exp. Cell Res.* **153**, 1 (1984); G. Sluder and C. L. Rieder, *J. Cell Biol.* **100**, 897 (1985).
2. G. Sluder, E. A. Thompson, F. J. Miller, J. Hayes, C. L. Rieder, *J. Cell Sci.* **110**, 421 (1997).
3. C. R. Brown, S. J. Doxsey, E. White, W. J. Welch, *J. Cell. Physiol.* **160**, 47 (1994); K. Fukasawa, T. Choi, R. Kuriyama, G. F. Vande Woude, *Science* **271**, 1744 (1996).
4. M. Winey, *Curr. Biol.* **6**, 962 (1996); G. A. Pihan *et al.*, *Cancer Res.* **58**, 3974 (1998).
5. R. E. Palazzo, E. Vaisburg, R. W. Cole, C. L. Rieder, *Science* **256**, 219 (1992).
6. E. H. Hinchcliffe, G. O. Cassels, C. L. Rieder, G. Sluder, *J. Cell Biol.* **140**, 1417 (1998).
7. G. Sluder, F. J. Miller, C. L. Rieder, *ibid.* **103**, 1873 (1986).
8. G. Sluder, F. J. Miller, R. Cole, C. L. Rieder, *ibid.* **110**, 2025 (1990); D. L. Gard, S. Hafezi, T. Zhang, S. J. Doxsey, *ibid.*, p. 2033.
9. R. S. Hartley, J. C. Sible, A. L. Lewellyn, J. L. Maller, *Dev. Biol.* **188**, 312 (1997).
10. K. R. Lacey, P. K. Jackson, T. Stearns, *Proc. Natl. Acad. Sci. U.S.A.*, in press.
11. A. Koff *et al.*, *Science* **257**, 1689 (1992); V. Dulic, E. Lees, S. I. Reed, *ibid.*, p. 1958.
12. R. Kuriyama and G. G. Borisy, *J. Cell Biol.* **91**, 814 (1982).
13. R. E. Rempel, S. B. Sleight, J. L. Maller, *J. Biol. Chem.* **270**, 6842 (1995).
14. G. Sluder and K. Lewis, *J. Exp. Zool.* **244**, 89 (1987); J. W. Raff and D. M. Glover, *J. Cell Biol.* **107**, 2009 (1988).
15. R. Balczon *et al.*, *J. Cell Biol.* **130**, 105 (1995).
16. A. W. Murray, *Methods Cell Biol.* **36**, 581 (1991).
17. Cycling *Xenopus* egg extracts were prepared as described (*16*) and used fresh. Demembranated sperm nuclei were prepared as described (*19*) and used at a final concentration of 400 heads/μl. Aphidicolin (Sigma) was added (final concentration of 10 μg/ml). Histone H1 kinase assays on egg extracts were done as described (*6*, *16*). Histone H1 phosphorylation was an-

alyzed by a phosphoimager (Molecular Dynamics, Sunnydale, CA) as described (*6*). To visualize asters, we placed extract in an FC-47 chamber [G. Sluder *et al.*, *Meth. Cell Biol.* **61**, 439 (1998)] and viewed it with a modified Zeiss ACM microscope (Zeiss) with polarization optics and a charge-coupled device camera (Hammamatsu, East Bridgewater, NJ, or Dage-MTI, Michigan City, IL) at 20°C. Time-lapse video images were written directly to the hard drive of a PC, as described (*6*). Video sequence playback of aster doubling was done with Adobe Premiere Software (Mountain View, CA).

18. S. Ikegami, S. Amemiya, M. Ouro, H. Nagano, Y. Mano, *Nature* **275**, 458 (1978).
19. M. Lohka and J. L. Maller, *J. Cell Biol.* **101**, 518 (1985); J. J. Blow and R. A. Laskey, *Cell* **47**, 577 (1986).
20. E. H. Hinchcliffe, C. Li, E. A. Thompson, J. L. Maller, G. Sluder, data not shown.
21. M. Dasso and J. W. Newport, *Cell* **61**, 811 (1990).
22. F. Tournier, M. Cyrklaff, E. Karsenti, M. Bornens, *Proc. Natl. Acad. Sci. U.S.A.* **88**, 9929 (1991); R. Heald *et al.*, *Nature* **382**, 420 (1996).
23. G. Sluder and C. L. Rieder, *J. Cell Biol.* **100**, 887 (1985).
24. J. Y. Su, R. E. Rempel, E. Erickson, J. L. Maller, *Proc. Natl. Acad. Sci. U.S.A.* **92**, 10187 (1995).
25. J. W. Harper and S. J. Elldrege, *Curr. Opin. Gen. Dev.* **6**, 56 (1996).
26. U. P. Strausfeld *et al.*, *J. Cell Sci.* **109**, 1555 (1996).
27. Glutathione S-transferase–tagged fusion proteins of Δ34Xic1 and C-Xic1 were prepared and purified as described (*13*, *24*). Recombinant *Xenopus* Cdk2-E complex was expressed, purified, and tested for kinase activity in vitro as described (*13*, *24*).
28. Immunofluorescence staining of *Xenopus* embryos was done as described (*8*), with affinity-purified polyclonal antibody to cyclin E (*9*) and monoclonal antibodies to α tubulin or γ tubulin (Sigma). Confocal microscopy was performed on an MRC-600 system (Bio-Rad, Hercules, CA). The confocal images presented represent projections of Z-series scans.
29. E. Bailly, J. Pines, T. Hunter, M. Bornens, *J. Cell Sci.* **101**, 529 (1992).
30. We thank F. J. Miller for help developing the observation chambers, C. Wilkerson and M. Cham for assistance in building the image acquisition computers, and R. Pope, T. Pederson, G. Witman, and B. Luna for comments on the manuscript. Supported by the NIH (J.L.M. and G.S.), the Trustees of the Worcester Foundation (G.S.), and the Cabot Family Charitable Trust (G.S.). J.L.M. is an investigator of the Howard Hughes Medical Institute. E.H.H. is supported by an NIH postdoctoral training fellowship. The authors would like to dedicate this work to the memory of Dan Mazia.

6 October 1998; accepted 12 January 1999

Mycolactone: A Polyketide Toxin from *Mycobacterium ulcerans* Required for Virulence

Kathleen M. George,[1] Delphi Chatterjee,[2] Geewananda Gunawardana,[3] Diane Welty,[1] John Hayman,[4] Richard Lee,[5] P. L. C. Small[1]*

Mycobacterium ulcerans is the causative agent of Buruli ulcer, a severe human skin disease that occurs primarily in Africa and Australia. Infection with *M. ulcerans* results in persistent severe necrosis without an acute inflammatory response. The presence of histopathological changes distant from the site of infection suggested that pathogenesis might be toxin mediated. A polyketide-derived macrolide designated mycolactone was isolated that causes cytopathicity and cell cycle arrest in cultured L929 murine fibroblasts. Intradermal inoculation of purified toxin into guinea pigs produced a lesion similar to that of Buruli ulcer in humans. This toxin may represent one of a family of virulence factors associated with pathology in mycobacterial diseases such as leprosy and tuberculosis.

Most pathogenic bacteria produce toxins that are important in disease. However, none has been identified for *Mycobacterium tuberculosis* and *Mycobacterium leprae*. The only mycobacterial pathogen for which there is any evidence of toxin production is *Mycobacteria ulcerans*, the causative agent of Buruli ulcer. Although Buruli ulcer is little known outside the tropics, it recently has been recognized as an emerging infection in western Africa (*1*). *Mycobacterium ulcerans* disease has several distinctive features. Infection results in progressive necrotic cutaneous lesions, which may persist for a decade if untreated and may extend to 15% of a patient's skin surface. Despite extensive necrosis, lesions are painless, symptoms of systemic disease are absent, and there is little histological evidence of an initial acute inflammatory response (*2*, *3*). Finally, in contrast to other pathogenic mycobacteria, which are facultative intracellular parasites of macrophages, *M. ulcerans* occurs in lesions primarily as extracellular microcolonies.

A curious feature of Buruli ulcer pathology is that organisms lie in a necrotic focus with the necrosis extending some distance from the site of bacterial colonization. This observation led to the hypothesis that *M. ulcerans* secreted a toxin (*2*). In 1974, Read *et al.* reported that a sterile filtrate of *M. ulcerans* had a cytopathic effect on cultured murine fibroblasts (*4*). Early efforts to isolate this toxin were not successful (*5*, *6*). More recently, Pimsler *et al.* (*7*) reported that a sterile filtrate of *M. ulcerans* had immunosuppressive properties. Earlier this year, we reported cytotoxic activity associated with acetone-soluble lipids (ASL) present in an organic extract from *M. ulcerans* sterile filtrate (*8*). The cytopathic effect of *M. ulcerans* or ASL on L929 murine fibroblasts was further characterized by showing that *M. ulcerans* or ASL arrested cells in the G_0/G_1 stage of the cell cycle. In this paper, we report the purification of this toxin and present evidence for its role in the pathogenesis of Buruli ulcer.

Initial attempts to obtain sufficient toxin from *M. ulcerans* sterile filtrate for structural analysis were frustrated by low yield. To increase yield, we developed a method for isolating toxin from intact bacteria (*9*). ASL were prepared from an extract of *M. ulcerans* containing chloroform and methanol (2:1) and were separated by thin-layer chromatography (TLC) on silica gel plates. Lipid bands were eluted from TLC plates and tested for cytopathicity on L929 mouse fibroblast cells as described (*8*). Maximum toxic activity was associated with a light yellow, ultraviolet-active component (*10*) with a refractive index of 0.23 in a solvent system containing chloroform, methanol, and water (90:10:1) (Fig. 1A). This compound was further purified by reversed-phase high-performance liquid chromatography and subjected to structural analysis. Mass spectral analysis of the toxin molecule under microspray conditions showed peaks at *m/z* 765 (strong), 743 (weak), and 725 (medium) (Fig. 1B). Accurate mass measurement of the peak at *m/z* 765 (M^+ + Na: $C_{44}H_{70}O_9Na$, observed 765.4912; calculated 765.4912; error <0.1 ppm) and the peak at *m/z* 725 (M^+-OH: $C_{44}H_{69}O_8$, observed 725.4988; calculated 725.4987; error = 0.1 ppm) gave the formula $C_{44}H_{70}O_9$ for the compound. The compound was identified by two-dimensional nuclear magnetic resonance spectral analysis as a polyketide-derived 12-membered ring macrolide (Fig. 2) (*11*). The toxin was named mycolactone to reflect its mycobacterial source and chemical structure.

To determine whether mycolactone was cytopathic, we applied serial dilutions of sterile filtrate or mycolactone to an overnight culture of L929 cells. Within 24 hours after addition of mycolactone, the cells rounded up and by 48 hours most cells lifted off the plate (Fig. 1C).

[1]Rocky Mountain Laboratories, National Institute of Allergy and Infectious Diseases, National Institutes of Health, Hamilton, MT 59840, USA. [2]Department of Microbiology, Colorado State University, Fort Collins, CO 80523-1677, USA. [3]Abbott Laboratories, Abbott Park, IL 60064, USA. [4]Box Hill Hospital, Box Hill, Victoria 3128 Australia. [5]National Institute of Allergy and Infectious Diseases, National Institutes of Health, Rockville, MD 20852, USA.

*To whom correspondence should be addressed. E-mail: psmall@nih.gov